forests

MDPI

Article

Online Measurement of Outline Size for *Pinus densiflora* Dimension Lumber: Maximizing Lumber Recovery by Minimizing Enclosure Rectangle Fitting Area

Min Ji, Wei Zhang *, Guofu Wang, Yong Wang and Hu Miao

Research Institute of Wood Industry, Chinese Academy of Forestry, Beijing 100091, China
* Correspondence: wzhang@caf.ac.cn

Abstract: This paper proposes a non-contact, online, rapid, and non-destructive measurement method of *Pinus densiflora S.et Z.* (*Pinus densiflora*) dimension lumber based on an algorithm of maximizing lumber recovery by minimizing the enclosure rectangle fitting area. The method takes the full influence of multiple factors, such as the difficulty in measuring large-size dimension lumber, conveying deflection, etc. into account. Image splicing, object and background segmentation, and lumber size measurements are carried out. Compared to other current algorithms, it can decrease the measurement errors and improve measurement efficiency. The problems of slow image segmentation, large-size lumber measurement, and conveying deflection are solved. Through measurement tests and error analysis, the measurement accuracy of the lumber size can reach 0.8 mm/m. This method meets the requirements of high-speed lumber production and lays the foundation for the development of a lumber detection and evaluation system.

Keywords: *Pinus densiflora*; lumber; outline size measurement; automatic vision system; dimensional measurement algorithm; object and background segmentation; deflection angle

check for updates

Citation: Ji, M.; Zhang, W.; Wang, G.; Wang, Y.; Miao, H. Online Measurement of Outline Size for *Pinus densiflora* Dimension Lumber: Maximizing Lumber Recovery by Minimizing Enclosure Rectangle Fitting Area. *Forests* **2022**, *13*, 1627. https://doi.org/10.3390/f13101627

Academic Editor: Paweł Kossakowski

Received: 6 September 2022
Accepted: 28 September 2022
Published: 3 October 2022

1. Introduction

Wood is mainly used as interior and exterior materials in residential and non-residential buildings [1]. *Pinus densiflora* is an important lumber species extensively used in in structural applications due to its abundance, desirable physical properties and its wide range of grades [2–5]. Therefore, the inspection requirements for *Pinus densiflora* dimension lumber are also very high, and the size and defects of the lumber are often important factors affecting the strength and performance of *Pinus densiflora* [6].

As one of the factors affecting the applications, the strength properties required in dimension lumber depends on its characteristics [7,8]. In the detection, measurement and grading of lumber, the use of the machine vision method has the advantages of high efficiency and accuracy. It can directly measure the size of the lumber by developing an algorithm with simple calculation and low hardware requirements. The size measurement of the dimension lumber is the basic work of defect detection, the dimension manufacturing process and material application [9]. Manual measurement using a steel tape, triangle ruler and a vernier caliper is a common size measurement method for dimension lumber. A Roller Measurement Instrument is installed for object length detection in some equipment, increasing the cost of sawn timber detection and grading [10]. This proposed method not only has accurate and stable detection results, but also has fewer restrictions, which is of great significance to the application of lumber for construction [11–13].

A size measurement system for wood production based on optical imaging was proposed. However, the research mainly dealt with the small size of images and focused on the influence of parameters and the discussion of algorithms. There was no discussion of the lighting, alignment, environmental conditions, and distortion effects [14]. Ergün et al. [15] applied a close range photogrammetric system to measure the dimension and shape of a

static object, but this operation was complex, the calculation was large, and the secondary development of the system was difficult. It did not use samples to verify the accuracy of the actual production and applications. The Harris algorithm is often used to detect the corner points of a similar chessboard image. This algorithm is subject to many interference points and is not suitable for dimension lumber because it is troublesome to deal with [16]. Sun et al. [17] compensated for the measurement results of the cylindrical gear profile by establishing a nonlinear model of perspective projection error. However, with respect to small-sized objects, as the size of the measuring object increases, the degree of lens distortion becomes larger and larger, and the compensation for one side in the measurement process alone cannot satisfy the accuracy requirement. The sheet measurement system consists of four measurement processes: image acquisition, camera calibration, extraction, and edges fitting. The total error of the system regarding the interference of the dimension lumber and the environmental conditions in the detection process are not analyzed [18].

In recent years, many scholars consider that the image edge is one of the most fundamental features of the image, which can be used to determine the size. In a complex recognition scene, it is important to accurately obtain the edge information of the target [19]. Roberts operator uses the local difference of the operator to find the image edge, and the calculation is simple but cannot suppress the noise effectively. A Sobel operator can smooth the noise, but the edge location accuracy is low [20]. The Canny operator performs non-maximum suppression and morphological connection operation, and gives the operator a strong denoising ability and a good edge detection effect, but the speed is very slow [21]. Wang et al. compared the performance of the previously mentioned algorithms, and the experimental results showed that there is no absolute superiority detection algorithm [22]. Roberts, Sobel, and Canny operators are used for the first or second derivative operator to locate the edge at the pixel level [23]. The improved detection algorithm can complete the optimal threshold value selection and edge detection process at the same time. However, the anti-noise performance, computational performance, and the real-time requirements still need to be improved [24]. In the last few years, the detection accuracy requirement has become higher and higher in the industry. The traditional pixel level edge detection cannot meet the actual needs, and sub-pixel edge detection accuracy is increasing [25]. Some scholars used the deep learning (DL) method to detect defects in wood products. To find objects that have not been trained before, it is necessary to train the neural network, and the adaptability of this method was poor [26]. The DL method is not suitable for large-size image recognition, but the length of dimension lumber is usually greater than 2 m. In recent years, although lots of 3D measurement methods have been proposed, many of them are applied to special fields and have limitations, and most existing methods are designed to measure small objects and are not suitable for large-size dimension lumber [27]. Optical three-dimensional measurement technology has certain requirements for the color and reflectivity of the object itself, the color of the object's surface is close, and the reflectivity of the object surface is uniform. However, a large number of objects with uneven absorption and reflectivity bring great challenges to optical three-dimensional measurements [28–31].

As the dimensional lumber is used for structural applications, the sizes and defects of the lumber are important factors affecting the strength properties. EN 14081-1 [32], EN 1912 [33] DIN 4074-1 [34] and other standards have high measurement and detection requirements for dimension lumber. Manual visual inspection and other detection technologies are gradually being replaced by machine vision technology. At present, the methods proposed by some scholars have a large amount of calculation, complex operation and difficult secondary development, and the measurement accuracy needs to be further improved. Further, the anti-interference performance and calculation speed still need to be improved [18]. In this study, the dimensional measurement of *Pinus densiflora* dimension lumber is carried out based on machine vision technology, and the error, accuracy and effect of the measurement are analyzed. It is desirable to find an algorithm that can extract the edge according to the characteristics of wood. This algorithm is accurate, simple, efficient, and low cost.

The proposed method has the advantages of being noncontact and high speed, and correlates well with linear scanning. This method can meet the high precision requirements of the dimension measurement of dimension lumber after being improved. With the help of more powerful computers, higher quality cameras and more precise sensors, measurement systems have the advantages of high measurement efficiency, low manual skill requirements, high precision, and low cost when measuring large-size *Pinus densiflora* dimension lumber, and it is expected that machine vision hardware and software will be applied at an industrial scale.

2. Materials and Methods

2.1. Materials

The Pinus densiflora trees were obtained from North Europe. The logs were sawn into lumber and all pieces of lumber were planed. We pre-selected sawn lumber without major defects in shape, but the surfaces of the lumber still had defects. In the experiment, the lumber length was 3985 mm, and the width was 150 mm. The surface of the lumber was taken as an example, and this algorithm was also suitable for thickness measurements of the lumber, and the moisture content of the tested dimension lumber was between 12%–15%. The factory application experiment was completed at Suzhou Crownhomes Co., LTD., Suzhou City, Jiangsu Province, China. The environment temperature of that day was 28 °C and the relative humidity was 63% (Figure 1).

Figure 1. The tested dimension lumber. (**a**) Research Institute of Wood Industry, Chinese Academy of Forestry (**b**) Dimension lumber.

2.2. Methods

A method for the measurement of lumber size was developed by C++ programming language, and OpenCV libraries were used to process the image and calculate the size of the lumber. The visual camera was used to scan the images of the lumber. The proposed algorithm was used to process the scanned images to realize the size measurement of the lumber.

2.2.1. The Image Splicing

In this study, the scan images of the pattern were grabbed by the line-scan camera and cool LED illumination in the uniform rectilinear motion state. Therefore, the image points were definitely matched with the space points on the pattern [35]. The Basler raL2048-48 gm line-scan camera with 2048 pixel per line resolution and 51 kHz line-scan rate was used. This camera was from the German Basler company, which was founded in 1988, has 30 years of experience in the field of vision technology, and is the world's leading computer vision expert. Because of the advantages of high resolution, high speed and real-time data acquisition, the LCD line-scan inspection has an efficient vision system. The exposure time of the line-scan camera can be controlled by making the exposure signal

from the composite of the signal from the encoder relate to the conveyer belt speed. So, the relative speed of the conveyor belt was detected by the speed sensor, and an online measurement of the outline size of the lumber can be obtained by the algorithm [36].

When the dimension lumber was measured using machine vision, the single picture taken by the line-scan camera only covered part of the lumber. It was necessary to stitch together multiple original pictures to restore the image of large-sized lumber. In view of the camera's short sampling time, a mismatch could occur as a result of the variance in adjacent image stitching data and the accumulation of errors [37]. Based on the area matching algorithm, an image splicing module was designed, which was fast, easy to implement, and highly applicable. The module included local image sampling→image sorting→coordinate mapping→image connection→image fusion.

The equation of positive relationship between the upper left corner and the lower left corner of the horizontal coordinate of the automatic splicing and fusion image is given in Equation (1):

$$R_1(i+1) = L_1(i) + W(i+1)\ i = 1, 2, 3 \ldots\ n \tag{1}$$

The equations of positive relationship between the upper left corner and the lower left corner of the vertical coordinates of the automatic splicing and fusion image are given in Equations (2) and (3):

$$L_2(j+1) = \mathrm{L}_2(j) + H(j+1)\ j = 1, 2, 3 \ldots\ n \tag{2}$$

$$R_2(j+1) = R_2(j) + H(j+1)\ j = 1, 2, 3 \ldots\ n \tag{3}$$

L_1 is the upper left horizontal coordinate of the lumber; R_1 is the upper right horizontal coordinate of the lumber; L_2 is the horizontal coordinate in the upper left corner of the current splicing image from top to bottom as the number of splices increases; R_2 is the vertical coordinates in the upper left corner of the current splicing from top to bottom as the number of splices increases; W is the pixel length of the splicing image; H is the pixel width of the splicing image; i is the sequence number of the splicing image in the horizontal direction. j is the sequence number of the splicing image in the vertical direction; n is the total number of images of the whole lumber.

The global splicing method worked as follows: Based on the upper and lower image registration algorithm, it was established that the displacement parameters $i = 0$ and $j = 0$. The vertical coordinate splicing was completed by mapping the column images from top to bottom onto the new coordinate of the image. The horizontal splicing was completed by mapping the row images from left to right onto the new coordinates. Based on the way the image was shot, only vertical splicing was needed, and the values of L_1, R_1 and W were fixed. The splicing was completed after the new vertical coordinates were mapped on (Figure 2).

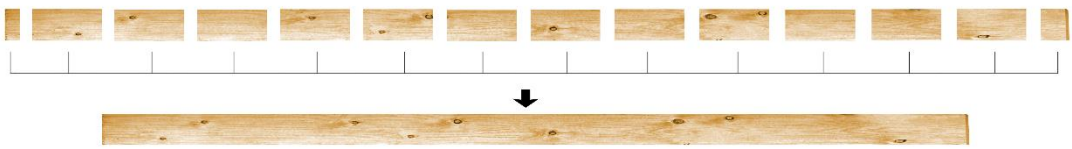

Figure 2. Process of automatic seamless splicing.

Manual splicing was not only time-consuming, but also prone to cause gaps in the splicing pictures, which led to inaccurate identification of the measurement of the lumber. Automatic splicing can solve the above two problems. It can accurately match the horizontal and vertical coordinates, and improve the recognition accuracy of lumber images.

2.2.2. Object and Background Segmentation Algorithm

A light source device was designed, which can automatically adjust the height and brightness. The device had a wide transverse radiation range and high brightness to

distinguish the object from the background better, reduce the error from the lumber edge detection, and improve the speed of image processing, which can overcome the influence of the environment on the capture of objects, and meet the requirements of high speed and large-format testing (Figure 3). By adjusting the appropriate light source, the surface and edge characteristics of the lumber can be clearly captured, which is conducive to the processing and analysis of the grayscale images [38]. The threshold segmentation of the lumber images before the application of the automatic adjusting light source device had a poor effect, and there was no good feature extraction for the lumber contour (Figure 4a). After the application of the automatic adjusting light source device, the threshold of the lumber and the background image was clearly segmented, which can characterize the edge characteristics of the lumber and improve the detection accuracy [39] (Figure 4b).

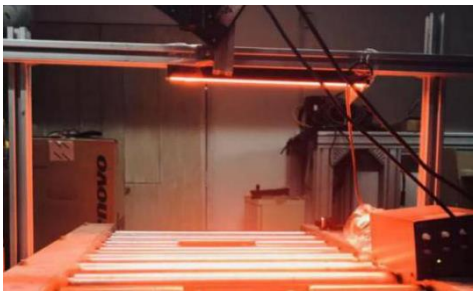

Figure 3. Automatic adjusting light source device.

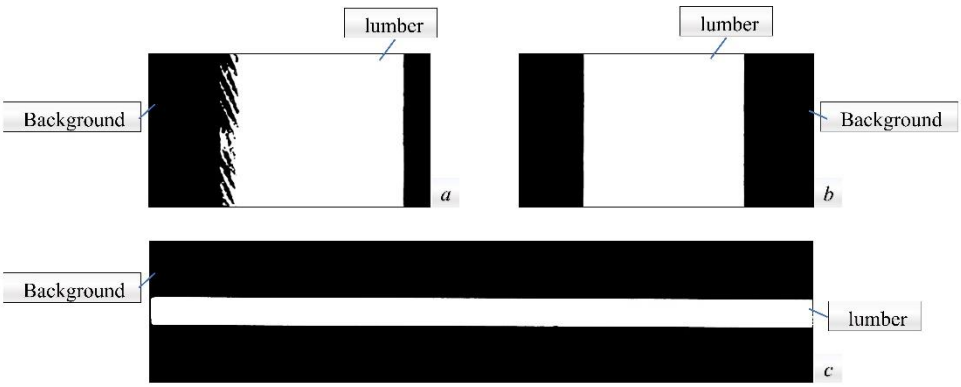

Figure 4. The image of threshold segmentation by applying the automatic adjusting light source device. (**a**) The image of threshold segmentation before applying the automatic adjusting light source device; (**b**) The image of threshold segmentation through applying the automatic adjusting light source device; (**c**) The lumber and background segmentation.

In terms of the software processing, binarization threshold segmentation and a median filtering algorithm were used to separate the lumber from the background. In consideration of the strong contrast between the lumber and the background and the grayscale characteristics of the image, median filtering and binarization processing were carried out, respectively [40]. Median filtering, a nonlinear filtering method, can remove impulse noise and small defects, and better retain the basic edge information of the image. In this experiment, the shape and size (nkernelSize) of the two-dimensional filtering window were set as 3. After the median filtering, the two-dimensional image matrix was outputted as 3×3 to prove $\boldsymbol{A}$. The center points $x_{i,j}$ were assigned the median of the nine pixel points. The local image (Figure 5) (pixel coordinates: $957 \leq x \leq 961$, $329 \leq y \leq 333$) of the digital matrix changes (Figure 5a) during the image processing. The central point $x_{i,j}$ (pixel coordinates $x = 959$, $y = 331$) was assigned 180 (Figure 5b). Finally, an appropriate threshold e was selected to divide the image pixels into groups. The image of the lumber segmented by binarization threshold was clear in the contour and defect, and a certain sharpness of the

edge was maintained to a certain extent. The digital matrix and the central point, $\boldsymbol{A}$ and $x_{i,j}$, are defined by Equations (4)–(6), respectively.

$$\boldsymbol{A} = \begin{bmatrix} x_{i-1,j-1} & x_{i-1,j} & x_{i-1,j+1} \\ x_{i,j-1} & x_{i,j} & x_{i,j+1} \\ x_{i+1,j-1} & x_{i+1,j} & x_{i+1,j+1} \end{bmatrix} \tag{4}$$

$$x_{i,j} = h \tag{5}$$

$$h = \frac{x_{i-1,j-1} + x_{i-1,j} + x_{i-1,j+1} + x_{i,j-1} + x_{i,j} + x_{i,j+1} + x_{i+1,j-1} + x_{i+1,j} + x_{i+1,j+1}}{3 \times 3} \tag{6}$$

187 (957,329)	177 (958,329)	191 (959,329)	174 (960,329)	177 (961,329)
183 (957,330)	180 (958,330)	184 (959,330)	172 (960,330)	175 (961,330)
184 (957,331)	180 (958,331)	188 (959,331)	177 (960,331)	178 (961,331)
183 (957,332)	176 (958,332)	187 (959,332)	178 (959,332)	176 (959,332)
181 (957,333)	176 (958,333)	187 (958,333)	177 (958,333)	183 (958,333)

a

187 (957,329)	177 (958,329)	191 (959,329)	174 (960,329)	177 (961,329)
183 (957,330)	180 (958,330)	184 (959,330)	172 (960,330)	175 (961,330)
184 (957,331)	180 (958,331)	180 (959,331)	177 (960,331)	178 (961,331)
183 (957,332)	176 (958,332)	187 (959,332)	178 (959,332)	176 (959,332)
181 (957,333)	176 (958,333)	187 (958,333)	177 (958,333)	183 (958,333)

b

Figure 5. Image digital matrix. (**a**) Image digital matrix before median filtering. (**b**) Image digital matrix after median filtering.

2.2.3. Dimensional Measurement Algorithm

As the edges of the contour images are not fully connected, it is necessary to assume that every internally connected segment in the image matrix is fully connected to identify the minimizing enclosure rectangle area. After that, the segments should be divided again. If there are disconnected parts, they should be marked as "connected", using as few pixels as possible. Finally, the minimum distance and area of the connected region were calculated [41].

During the image acquisition, the running direction of the lumber can be controlled by setting an automatic adjustment baffle for the width of the lumber on the roller table. However, both the operation of the lumber on the roller table and the image acquisition by the line-scan would be affected when the width is too short. This would lead to a deviation in image acquisition, and then further affect the fitting accuracy of the dimension. The minimum enclosure rectangle boundary rotation algorithm can not only meet the measurement requirements, but also improve the accuracy of length and width measurements, as well as accelerate the calculation.

The upper left corner of the image was taken as the origin of coordinates, and then the boundary endpoints of the minimum enclosure rectangle p [0], p [1], p [2] and p [3], and its length and width were determined (Figure 6). In this way, the length, width, circumference, and area of all the minimum enclosure rectangles in the segmented images can be calculated. The point with the maximum value on the y-axis of the minimum enclosure rectangle is p [0], and the distance between p [1], p [2] and p [3] is determined clockwise. The distance between p [0] and p [3] is determined as the length, and the distance between p [0] and p [2] is determined as the width.

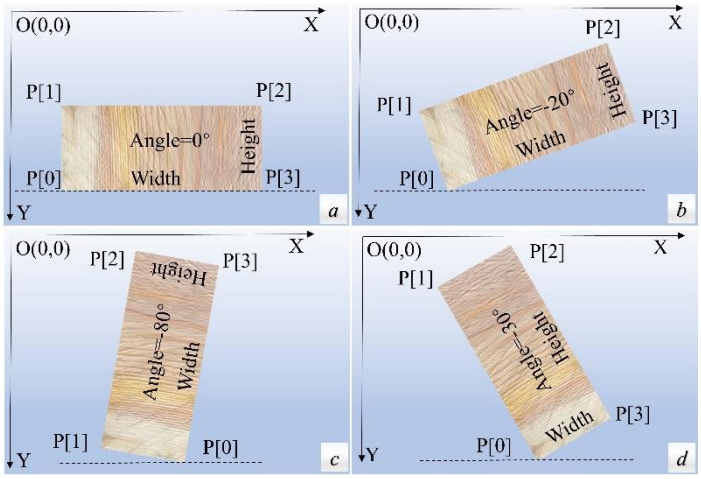

Figure 6. The minimum enclosure rectangle fitting in the case of rotation. (**a**) Angle = 0° (**b**) Angle = −20° (**c**) Angle = 80° (**d**) Angle = −30°.

The center point of the minimum enclosure rectangle was taken as the rotation coordinate point, and the coordinate was set as (x_i, y_i). The coordinate of $p[j]$ (j-th point on the boundary of the minimum enclosure rectangle) was set as (x_j, y_j). Hence the equation of the rotation angle φ_j (calculate as the included angle between the boundary of the minimum enclosure rectangle and the X-axis counterclockwise) is given in Equation (7):

$$\varphi_j = \arctan\left(\frac{y_j - y_i}{x_j - x_i}\right) \tag{7}$$

Affine transformation mainly includes translation, scale, flip, rotation, and shear. Rotation transformation in the affine transformation is mainly used to reduce conveying defection error in the measurement of lumber. The center point of the minimum enclosure rectangle was set as the rotation coordinate point $p[i]$ and rotated clockwise by the angle of φ_j around the rotation point $p[i]$ successively. Based on the spatial affine rotation transformation, the transformation matrix and transformation inverse matrix are defined by Equations (8) and (9), respectively.

$$\boldsymbol{M} = \begin{bmatrix} \cos\varphi_j & \sin\varphi_j & 0 \\ -\sin\varphi_j & \cos\varphi_j & 0 \\ 0 & 0 & 1 \end{bmatrix} \tag{8}$$

$$\boldsymbol{M}^{-1} = \begin{bmatrix} \cos\varphi_j & -\sin\varphi_j & 0 \\ \sin\varphi_j & \cos\varphi_j & 0 \\ 0 & 0 & 1 \end{bmatrix} \tag{9}$$

Assume that the coordinates of the minimum enclosure rectangle boundary point $p[j]$ are (x_j, y_j), and after the rotation, the coordinates turn into $\left(\vec{x_j}, \vec{y_j}\right)$. The equation of rotation is given in Equation (10):

$$\begin{bmatrix} \vec{x_j} \\ \vec{y_j} \end{bmatrix} = \begin{bmatrix} \cos\varphi_j & \sin\varphi_j \\ -\sin\varphi_j & \cos\varphi_j \end{bmatrix} \begin{bmatrix} x_j \\ y_j \end{bmatrix} \tag{10}$$

The equation of reverse rotation is given in Equation (11):

$$\begin{bmatrix} x_j \\ y_j \end{bmatrix} = \begin{bmatrix} \cos\varphi_j & -\sin\varphi_j \\ \sin\varphi_j & \cos\varphi_j \end{bmatrix} \begin{bmatrix} \vec{x_j} \\ \vec{y_j} \end{bmatrix} \tag{11}$$

After noting down the area of the current lumber, it was compared with the previous one. If it is greater than the previous value, the previous value remains; if it is smaller, the previous one is replaced by the current area of the minimum enclosure rectangle (Figure 7a).

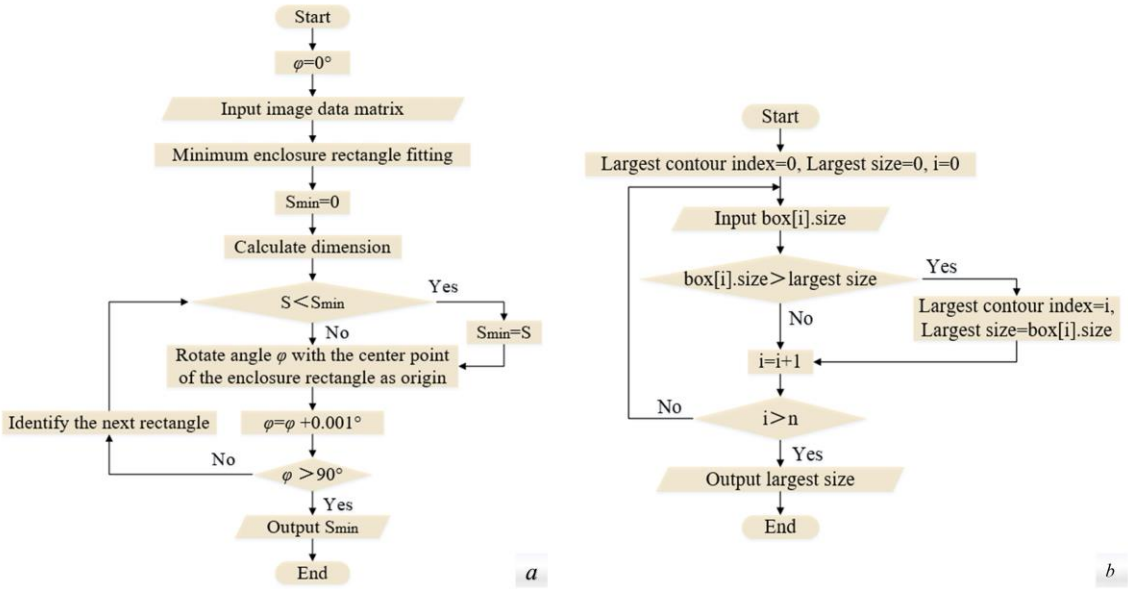

Figure 7. Flowchart of dimensional measurement. (**a**) The minimum enclosure rectangle fitting. (**b**) The algorithm of maximum size search.

However, because of the interference of other factors, such as the surface defects of the dimension lumber, the sawn edge, and the excessive exposure to light (Figure 8), the minimum enclosure rectangle on the image contains more than the result of the size of the lumber. Hence, it is necessary to adopt the search method of maximum size value to remove all the other irrelevant values of the minimum enclosure rectangle [42]. The image object collected by the system is the lumber, and it is the largest enclosure rectangle in the image. This study improved the minimum enclosure rectangle algorithm and selected the maximum length and width in all the identified rectangles, namely the length and width of the lumber (Figure 7b). *i* is the *i*-th identified minimum enclosure rectangle, and *n* is the total number of the identified minimum enclosure rectangles in the image.

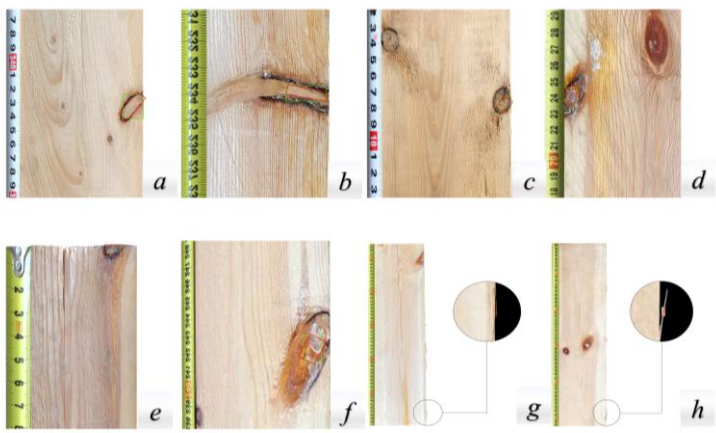

Figure 8. The interference factors on the measurement of the minimum enclosure rectangle of lumber: (**a**) type: spike knot; (**b**) type: spike knot; (**c**) type: round knot; (**d**) type: round knot; (**e**) type: end knot; (**f**) type: end knot; (**g**) type: rough saw cut; (**h**) type: rough saw cut.

2.2.4. The Size of Calibration

The system uses different methods to convert pixels into dimensions in the transverse and longitudinal directions, and the minimum unit of the output size is 0.01 mm. According to the triangular projection relation, the actual size of the lumber corresponding to the transverse pixels of the image is related to its optical path position. Therefore, to achieve the highest accuracy with dimension measurement, it is necessary to use piecewise functions to obtain the corresponding dimensions of each horizontal feature pixel, W_x, which is defined by Equation (12) [43].

$$W_x = Q(D_x) - Q(D_0) = K_1 \times P_x \tag{12}$$

D_x is the horizontal pixel position on the right of the lumber to be measured. D_0 is the horizontal pixel position of the original point.

Suppose D_x is the pixel position of the n-th segment, the transverse interval piecewise function, $Q(D_x)$, is defined by Equation (13).

$$Q(D_x) = \sum_{i=0}^{n-1} w(i) + f(n, D_x) \tag{13}$$

The linear speed transmitted by the roller table of this system is accurately measured through the pulse number of the encoder, and the scanning speed of the camera is controlled by the pulse excitation of the encoder. When it comes to the longitudinal dimension calibration, K_2 is the ratio of the length of the feature pixel points to the actual length of the lumber; the longitudinal dimension of the lumber, H_y, is defined by Equation (14).

$$H_y = Q(D_y) - Q(D_0) \tag{14}$$

D_y is the vertical pixel position on the left bottom of the lumber that is to be measured; D_0 is the longitudinal pixel position of the original point.

Suppose D_y is the pixel position of the n-th segment, the longitudinal interval piecewise function, $Q(D_x)$, is defined by Equation (15):

$$\mathrm{Q}(Dy) = \sum_{i=0}^{n-1} h(i) + f(n, Dy) \tag{15}$$

In the actual measurement, the length and width of the lumber are not completely aligned with the horizontal and vertical axis due to conveying deflection during the image acquisition. When the lumber is affected by conveying deflection, the main axis of the object should be determined firstly, and then the length and width of the object (the enclosure rectangle) along the main axis direction should be identified to identify the minimum area of the enclosure rectangle. Suppose the horizontal coordinates of the rectangles are $D_x(x_1, y_1)$ and $D_0(x_0, y_0)$, respectively. After image splicing, the target object is identified by the minimum enclosure rectangle. The corresponding size of the width feature pixel W_{MERx} is defined by Equation (16).

$$W_{MERx} = K_1\sqrt{(y_1 - y_0)^2 + (x_1 - x_0)^2} \tag{16}$$

K_1 is the ratio of the width of the feature pixels to the actual width of the lumber.

It is assumed that the ordinates of the lumber are $D_y(x_2, y_2)$ and $D_0(x_0, y_0)$, respectively. After image splicing, the minimum enclosure rectangle was identified on the target object. The corresponding size of the width feature pixel H_{MERy} is defined by Equation (17).

$$W_{MERx} = K_2\sqrt{(y_1 - y_0)^2 + (x_1 - x_0)^2} \tag{17}$$

K_2 is the ratio of the length of the feature pixels to the actual length of the lumber.

The camera's intrinsic and extrinsic parameters were evaluated by utilizing a piece of 18 × 22 checkerboard to calibrate the camera, and the camera lens distortion was also considered to ensure the accuracy of the dimensional measurements. The checkerboard image was used to calibrate the ratio (K_1 K_2) of the length of the lumber to its width. Excluding the influence of other factors, the smaller the rotation angle, the more accurate the measurement results. The experiment results showed that K_1 = 19.608, and K_2 = 8.529. Equipped with a length roller measurement instrument in the length measurement direction, when the results differ greatly from the machine vision results, the system would suggest re-measurement.

2.2.5. Statistical Analysis

In order to verify the feasibility of the dimensional measurement technology, the measured length and width of the lumber was compared to the actual measurements. The actual data of the lumber measured using a steel tape (accuracy of 1 mm), triangle ruler (accuracy of 1 mm) and a vernier caliper (accuracy of 0.01 mm) was taken as the reference standard value. So as to evaluate the measurement accuracy and measurement error, Bias, relative Bias, root mean square error (RMSE) and relative mean square error (rRMSE) were used to evaluate the measurement accuracy of the algorithm based on the machine vision [44].

$$Bias = \frac{1}{n}\sum_{i=1}^{n} e_i = \frac{1}{n}\sum_{i=1}^{n}(y_i - y_{ri}) \tag{18}$$

$$rBias = \frac{|Bias|}{\overline{y_r}} \times 100\% \tag{19}$$

$$rBias = \frac{Bias}{\overline{y_r}} \times 100\% \tag{20}$$

$$RMSE = \sqrt{\frac{\sum (y_i - y_{ri})^2}{n}} \tag{21}$$

$$rRMSE = \frac{RMSE}{\overline{y_r}} \times 100\% \tag{22}$$

where y_i is the measured value based on machine vision, y_{ir} is the actual reference standard value, n is the number of samples, and $\overline{y_r}$ is the actual measured mean; the above four evaluation indexes were used to evaluate the measurement accuracy.

3. Results

3.1. Deflection Angle and Error

The green rectangle is the initial minimum enclosure rectangle. The dimension lumber is rotated around the center point to the horizontal position to identify the enclosure rectangle. Then, the dimension lumber is rotated back to the initial position. The minimum enclosure rectangle is shown as the red rectangle in Figure 9. The identification of the minimum enclosure rectangle of the lumber in different angles (0.28°–5.44°) is shown in Figure 9. From the perspective of area compensation, the greater the deflection angle, the greater the rectangle identification area to be corrected.

Compare the length and width of the minimum enclosure rectangle without the rotation algorithm with that of the improved rotation algorithm (the actual length of 458.50 mm and the width of 48.00 mm), the inaccuracy of the length decreased by 0.188%–0.469%, and the inaccuracy of the width decreased by 15.450%–191.522% (Table 1). Eventually, the length, width, circumference, and area of the lumber can be measured. The error of the measurement result can be narrowed within 0.8 mm per meter (Table 2). It can be concluded that this algorithm can solve the problem of conveying deflection well, improve the fitting accuracy of the lumber, and minimize the deviation caused by conveying deflection.

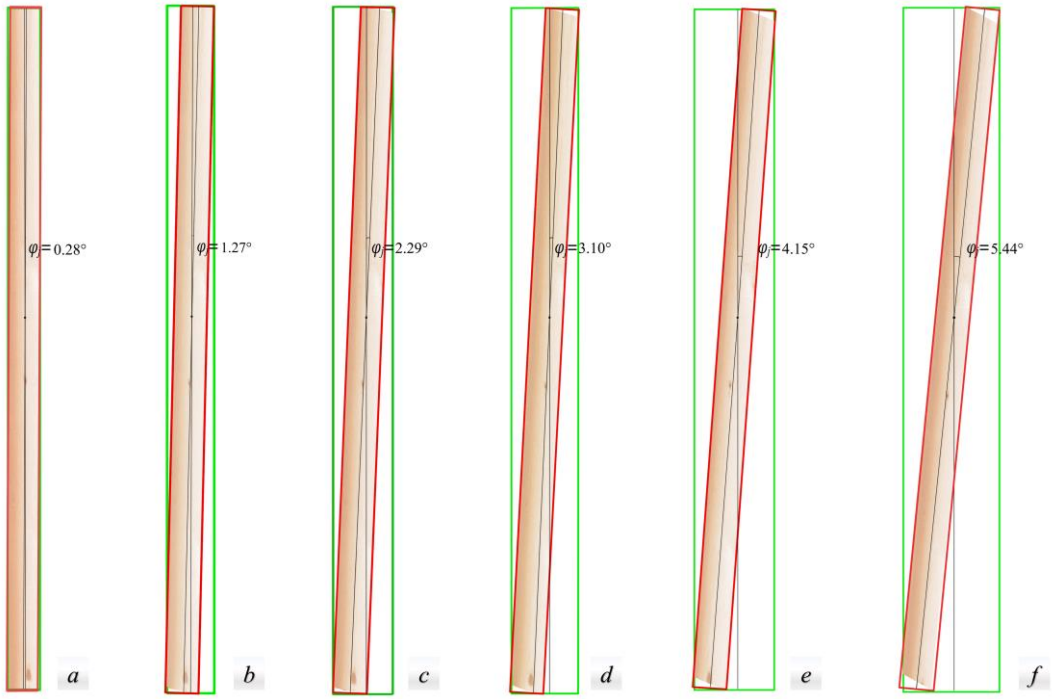

Figure 9. Fitting of the minimum enclosing rectangle before and after the rotation of the dimension lumber with different conveying deflection angles. (**a**) deflection angle φ_j = 0.28°; (**b**) deflection angle φ_j = 1.27°; (**c**) deflection angle φ_j = 2.29°; (**d**) deflection angle φ_j = 3.10°; (**e**) deflection angle φ_j = 4.15°; (**f**) deflection angle φ_j = 5.44°.

Table 1. Dimensional measurement of dimension lumber in different conveying deflection angles.

Deflection Angle/°	Measured Length/mm	Measured Width/mm	Measured Circumference/mm	Measured Area/mm^2
0.28	460.011	50.004	1033.770	22,835.733
1.27	460.104	50.007	1030.701	22,798.58
2.29	460.155	50.009	1051.271	23,038.381
3.10	460.207	50.012	1047.036	22,681.396
4.15	460.258	50.018	1041.482	22,663.985
5.44	460.309	50.023	1060.413	22,861.272

As can be seen from the data in Table 2, the percent error of the width measurement was significantly reduced, and that of the length measurement was also reduced to a certain extent. This means that the improved algorithm can accurately identify the rotating rectangle and reduce the error, so as to improve measurement accuracy.

The linear function fitting deflection angle and percentage reduction in width detection error is $y = 32.527x + 3.728$, $R^2 = 0.9982$ (Figure 10a). The linear function fitting deflection angle and percentage reduction in the length detection error before 1 degree (deflection angle, x axis) is $y = 0.166x + 0.144$, $R^2 = 0.9546$; The linear function fitting deflection angle and percentage reduction in the length detection error after 1 degree (deflection angle, x-axis) is $y = 0.049x - 0.235$, $R^2 = 0.8859$ (Figure 10b). As the deflection angle increases, the percent error of the length and width measurements increase. The structural sawn timber can effectively reduce the deflection detection error of the large-size dimension lumber within the above deflection angle range, thereby increasing measurement accuracy. In practice, the general conveying deflection angle is within 5°, and a greater than 5° has no research significance, and is usually not discussed.

Table 2. Comparison between the measurements based on machine vision and the actual measurements.

Deflection Angle/°	Size	rBias (before Rotation)/%	rBias (after Rotation)/%	rRMSE (before Rotation)/%	rRMSE (after Rotation)/%	Percentage Reduction in Error/%
0.28	length	0.190	0.002	0.134	0.002	0.188
	width	15.457	0.007	10.930	0.005	15.450
1.27	length	0.358	0.023	0.253	0.016	0.335
	width	49.415	0.014	34.941	0.010	49.400
2.29	length	0.413	0.034	0.292	0.024	0.380
	width	85.480	0.019	60.444	0.013	85.461
3.10	length	0.436	0.045	0.308	0.032	0.390
	width	127.400	0.023	90.086	0.017	127.377
4.15	length	0.492	0.056	0.348	0.040	0.436
	width	157.611	0.035	111.448	0.025	157.576
5.44	length	0.536	0.067	0.379	0.048	0.469
	width	191.569	0.047	135.460	0.033	191.522

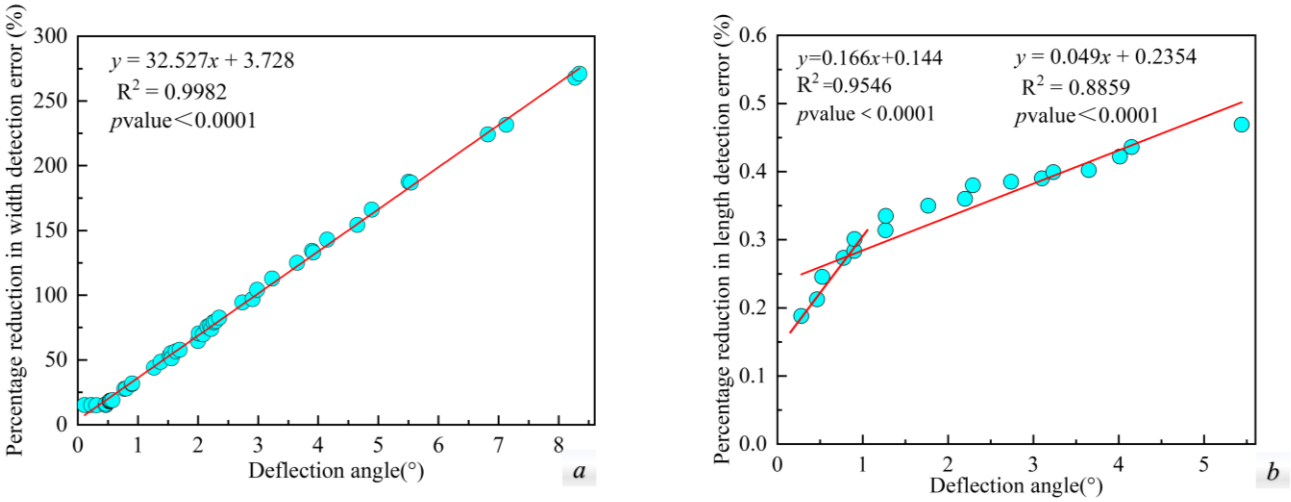

Figure 10. Percentage reduction in error of the dimensional measurement (%). (**a**) Percentage reduction in error of the width measurement (%). (**b**) Percentage reduction in error of the length measurement (%).

3.2. Numerical Analyses

The length and width were measured at different positions on the dimension lumber, and the average values were taken as the actual dimensions of the lumber. The average size of the six test samples were 3985.333 mm × 149.667 mm, 3986.167 mm × 149.667 mm, 3985.167 mm × 150.500 mm, 3985.167 mm × 150.000 mm, 3985.667 mm × 150.833 mm, and 3985.500 mm × 150.333 mm. The scanning and measurements were carried out six times for the lumber, and the average value of the six measurements was used for further calculations.

In the industrial experiments, the length, width, circumference, and area of the dimension lumber were measured based on machine vision. It can be seen in Table 3 that the measured value is similar to the actual size, and that the size of the lumber can be accurately identified within the allowable error range. As can be seen in Table 4, the range of length Bias is −0.421 mm–2.016 mm; the range of width Bias is −0.034 mm–0.101 mm; the range of length rBias is 0.011%–0.051%; the range of width rBias is 0.004%–0.067%; the length RMSE range is 0.297 mm–1.425 mm; the width RMSE range is 0.004 mm–0.071 mm; the length rRMSE range is 0.007%–0.036%; and the width rRMSE range is 0.003%–0.047%. The results show that the measured value is reliable and can meet the precision requirements of dimensional measurement of large-size dimension lumber.

Table 3. Dimensional measurement of *Pinus densiflora* the dimension lumber.

Samples	Measured Length/mm	Measured Width/mm	Measured Circumference/mm	Measured Area/mm^2
1	3987.349	149.659	8992.908	566,763.835
2	3985.543	149.725	8738.467	565,252.826
3	3984.150	150.601	8625.958	566,452.072
4	3984.746	150.083	8622.971	563,868.548
5	3984.135	150.799	8674.624	564,118.942
6	3983.736	150.327	8958.893	569,050.205

Table 4. The error analysis of the dimensional measurement of the lumber.

Samples	Size	Bias/mm	rBias/%	RMSE/mm	rRMSE/%
1	length	2.016	0.051	1.425	0.036
	width	0.008	0.005	0.005	0.004
2	length	0.623	0.016	0.441	0.011
	width	0.058	0.039	0.041	0.028
3	length	1.017	0.026	0.719	0.018
	width	0.101	0.067	0.071	0.047
4	length	0.421	0.011	0.297	0.007
	width	0.083	0.055	0.058	0.039
5	length	1.532	0.038	1.083	0.027
	width	−0.034	0.023	0.024	0.016
6	length	1.764	0.044	1.247	0.031
	width	−0.007	0.004	0.004	0.003

The experiments show that the precision of the measuring system can be controlled within 0.8 mm per meter, as shown in Table 4, which satisfies the accuracy of dimensional measurement of large-size dimension lumber in the industry, which have high application value as building materials. Due to the tolerance in sawing and shrinkage variation of the lumber affecting the measurement results, the lumber is not a completely regular rectangular circumference and area. In some saw mills, lumber size is often calculated by its length and width, which is not accurate. In this paper, a method of measuring the circumference and area of the dimension lumber based on the pixel proportion algorithm is proposed, which can effectively, conveniently, and accurately measure the circumference and area of *Pinus densiflora* dimension lumber.

4. Discussion

A scan image of *Pinus densiflora* dimension lumber is grabbed by the Basler line-scan camera, analyzed by the improved algorithm, and uses an automatic adjusting light source device. The advanced algorithm effectively improves the detection efficiency and detection accuracy. This noncontact and nondestructive testing measurement system meets the needs of the sawmills.

High accuracy 3D measurements based on the 2D sensor platform within the scope of the cost should be addressed in future work [45]. Combined with the multi-sensor technology, it solves the problems existing in current 3D measurement technology in the measurement of dimension lumber, and integrates laser and CMOS (Complementary Metal-Oxide-Semiconductor) technology to achieve a high precision dimension measurement. The detection system can not only be used for both longitudinal and transversal sawing lines, but may also be seamlessly integrated into any existing production line [46].

The main advantage of this system using a 2D measurement, is that the dimension lumber is fully scanned. Movements of the lumber would not have any influence on the dimensional measurement, which could generate more secure measurements and more stable signals as compared to older systems based on the 1D measurement technique. The whole system reduces moving parts, reduces mechanical wear, and has durable vision, being easy

to install in new and existing production lines [47]. The system can be equipped with the advanced technology that allows bent and twisted lumber with different thicknesses to be reliably measured.

Dimension lumber distortion following changing moisture content may lead to a high rejection rate in lumber grading and construction applications. In the future, this method, based on machine vision, will be able to provide full field measurements with high resolution. The method can identify the slight shrinkage changes of lumber and judge the shrinkage of wood over a certain range. This method can be used to measure shrinkage properties of softwood species [48].

The measurement of structural lumber using machine vision is a cutting-edge technology in the application of the wood processing industry. In future, it is expected that further research will be carried out on wood defect identification, optimal production, quality evaluation and the applications of *Pinus densiflora* structural lumber [49].

A self-triggering function to start the measurement should also be addressed in future work. This system has a range masking feature, which eliminates measurement deterioration due to reflections from surrounding equipment. A measurement algorithm that can distinguish between object and background and has a high measurement rate will secure a high turning efficiency [50].

5. Conclusions

By adding the automatic adjusting light source device, the scan image can be flexibly adjusted and adapted to the illumination conditions influenced by the detection environment, allowing for the *Pinus densiflora* lumber surface color, texture, and other properties to be identified.

The fusion image splicing algorithm is developed for the identification of large-size *Pinus densiflora* dimension lumber, which can reduce identification error, save manual splicing time, speed up image processing, and solve the problems of misidentification. This will be well regarded by engineers and builders, especially for structural components and heavy timber applications.

The feature extraction of the dimension lumber can be effectively realized, and the inaccuracy of edge recognition caused by interferences can be solved. After different processing images and digital matrixes are compared, it has been proven that the algorithm can achieve a good segmentation effect of the object and background.

The improved minimum enclosure rectangle algorithm can solve the problem of the deflection error of the dimension lumber affecting the fitting accuracy. Through the experiments, the linear relationship between the deflection angle and the percentage decrease in length and width measurement errors are proved in the deflection angle range of 5°. The results show that the identification error can be reduced using the minimum enclosure rectangle rotation algorithm. When the minimum enclosure rectangle of identification error appears in the image, combined with the maximum search method, the length, width, circumference, and area of the dimension lumber are output, and other misidentification interferences are eliminated. Using the pixel proportion method to obtain the circumference and area values of the dimension lumber can accurately measure the size of the dimension lumber. The algorithm is simple, fast, and accurate, which can solve the existing problems. It has important application significance in sawmills and building materials. This study verifies the reliability and stability of the system through the factory test and data analysis, which has important production and application values.

Author Contributions: Methodology M.J., W.Z. and Y.W.; Resources M.J. and W.Z; Experiments M.J., G.W. and H.M.; Analysis M.J. and W.Z.; Roles & Writing—original draft M.J.; Writing—review & editing W.Z.; Validation G.W. All authors have read and agreed to the published version of the manuscript.

Funding: This work was supported by the Program of Forestry Science and Technology Promotion Project of the State Forestry and Grassland Administration of China (Grant No. [2019]35), National Natural Science Foundation of China (CN) (Grant No. 31670721) and Key Project and Discipline Project of the Chinese Academy of Forestry (Grant No. CAFYBB2018ZB011).

Conflicts of Interest: The authors declare that they have no known competing financial interests or personal relationships that could have appeared to influence the work reported in this paper.

References

1. Seo, H.J.; Kim, N.K.; Jo, J.M.; Lee, M.C. Fire properties of pinus densiflora utilizing fire-retardant chemicals based on borate and phosphorus (II)–thermal and gas emission characteristics. *BioResources* **2018**, *13*, 5417–5427. [CrossRef]
2. JiYoung, A.; JeiWan, L.; KyungNak, H. Genetic Diversity and Structure of Pinus densiflora Siebold & Zucc. Populations in Republic of Korea Based on Microsatellite Markers. *Forests* **2021**, *12*, 750–764.
3. Park, J.; Kim, W.; Kim, W.; Park, C.; Choi, C.Y.; Cho, J.; Kim, S.; Cheong, H. Antihypertensive Effects of Dehydroabietic and 4-Epi-Trans-Communic Acid Isolated from Pinus densiflora. *J. Med. Food* **2021**, *24*, 50–58. [CrossRef] [PubMed]
4. Lee, C.S.; Chun, Y.M.; Lee, H.; Pi, J.H.; Lim, C.H. Establishment, regeneration, and succession of Korean red pine (*Pinus densiflora* S. et Z.) Forest in Korea. In *Conifers*; IntechOpen: London, UK, 2018.
5. Purusatama, B.D.; Kim, N.H. Cross-field pitting characteristics of compression, lateral, and opposite wood in the stem wood of Ginkgo biloba and Pinus densiflora. *IAWA J.* **2020**, *41*, 48–60. [CrossRef]
6. Park, C.; Lee, U.; Kim, S.; Lee, K. The Relationship between Tree-Ring Growths of Pinus densiflora and Climate from Three Mountains in Central Region, the Republic of Korea. *Atmosphere* **2021**, *12*, 878. [CrossRef]
7. Hyuk, J.J.; Min, L.; Min, L.S.; Bum, P.S. Formaldehyde Emission of Building Materials and Effect of Carbonized Board on Their Reduction. *J. Korean Wood Sci. Technol.* **2017**, *45*, 327–334.
8. Kandler, G.; Lukacevic, M.; Füssl, J. An algorithm for the geometric reconstruction of knots within timber boards based on fibre angle measurements. *Constr. Build. Mater.* **2016**, *124*, 945–960. [CrossRef]
9. Zhao, J.; Meng, Z.; Jin, Z.; Chen, D.; Wu, Y.; Zhang, W. Bending properties of bamboo scrimber with holes in different sizes and positions. *Constr. Build. Mater.* **2019**, *200*, 209–217. [CrossRef]
10. Buck, R.A.; Buehlmann, U.; Thomas, R.E. ROMI-3.1 Least-Cost Lumber Grade Mix Solver Using Open Source Statistical Software. *For. Prod. J.* **2010**, *60*, 432–439. [CrossRef]
11. Hu, J.; Song, W.; Zhang, W.; Zhao, Y.; Yilmaz, A. Deep learning for use in lumber classification tasks. *Wood Sci. Technol.* **2019**, *53*, 505–517. [CrossRef]
12. Brunetti, M.; Burato, P.; Cremonini, C.; Negro, F.; Nocetti, M.; Zanuttini, R. Visual and machine grading of larch (Larix decidua Mill.) structural timber from the Italian Alps. *Mater. Struct.* **2016**, *49*, 2681–2688. [CrossRef]
13. Yang, S.; Park, Y.; Chung, H.; Kim, H.; Park, S.; Choi, I.; Kwon, O.; Yeo, H. Soft Independent Modeling of Class Analogy for Classifying Lumber Species Using Their Near-infrared Spectra. *J. Korean Wood Sci. Technol.* **2019**, *47*, 101–109. [CrossRef]
14. Funck, J.W.; Gaber, J.A.; Aslam, F. Using image analysis for lumber size control measurements. *Ind. Metrol.* **1992**, *2*, 237–252. [CrossRef]
15. Ergün, B. An expert measurement system for photogrammetric industrial application. *Measurement* **2006**, *39*, 415–419. [CrossRef]
16. Qiao, Y.; Tang, Y.; Li, J. Improved Harris sub-pixel corner detection algorithm for chessboard image. In Proceedings of the 2013 2nd International Conference on Measurement. Information and Control, Harbin, China, 16–18 August 2013; pp. 1408–1411.
17. Sun, Z.; Xu, Z.P.; Wang, Y.Q. Control and compensation of perspective projection error analysis in machine vision measurement. *Comput. Eng. Appl.* **2018**, *54*, 266–270.
18. Geng, L.; Yao, F.; Wang, W.; Xi, J.; Li, Y. Error compensation method of largre-size steel sheet measurement based on control field. *J. Phys. Conf. Ser.* **2019**, *1213*, 042025. [CrossRef]
19. Duan, R.; Li, Q.; Li, Y.Y. Summary of image edge detection. *Opt Tech* **2005**, *3*, 415–419.
20. Kumar Singh, R.; Shekhar, S.; Bhawan Singh, R.; Chauhan, V. A comparative study of edge detection techniques. *Int. J. Comput. Appl.* **2014**, *100*, 5–8.
21. Prasad, R.; Suresh, S. A review on edge detection algorithms. *IJMCA* **2016**, *4*, 7–11.
22. Wang, Z.W. Comparison research of capability of several detection operators for edge detection. *Manuf Autom.* **2012**, *11*, 6.
23. Vijaya Kumar Reddy, R.; Prudvi Raju, K.; Jogendra Kumar, M.; RaviKumar, L.; Ravi Prakash, P.; Sai Kumar, S. Comparative analysis of common edge detection algorithms using pre-processing technique. *Int. J. Electr. Comput. Eng.* **2017**, *7*, 2574–2580. [CrossRef]
24. Xie, X.; Ge, S.; Xie, M.; Hu, F.; Jiang, N. An improved industrial sub-pixel edge detection algorithm based on coarse and precise location. *J. Ambient. Intell. Humaniz. Comput.* **2020**, *11*, 2061–2070. [CrossRef]
25. Chen, Q.C.; Hou, Y.Q.; Tan, Q.C. A subpixel edge detection method based on an arctangent edge model. *Optik* **2016**, *127*, 5702–5710.

26. Wang, Y.; Zhang, W.; Gao, R.; Jin, Z.; Wang, X. Recent advances in the application of deep learning methods to forestry. *Wood Sci. Technol.* **2021**, *55*, 1171–1202. [CrossRef]
27. Shi, J.; Sun, Z.; Bai, S. Large-scale three-dimensional measurement via combining 3D scanner and laser rangefinder. *Appl. Opt.* **2015**, *54*, 2814–2823. [CrossRef]
28. Liang, J.; Gu, X. Development and application of a non-destructive pavement testing system based on linear structured light three-dimensional measurement. *Constr. Build. Mater.* **2020**, *260*, 119919. [CrossRef]
29. Wang, J.; Zhou, Y.; Yang, Y. A novel and fast three-dimensional measurement technology for the objects surface with non-uniform reflection. *Results Phys.* **2020**, *16*, 102878. [CrossRef]
30. Gao, Y.; Cheng, T.; Su, Y.; Xu, X.; Zhang, Y.; Zhang, Q. High-efficiency and high-accuracy digital image correlation for three-dimensional measurement. *Opt. Lasers Eng.* **2015**, *65*, 73–80. [CrossRef]
31. Purusatama, B.D.; Choi, J.K.; Lee, S.H.; Kim, N.H. Microfibril angle, crystalline characteristics, and chemical compounds of reaction wood in stem wood of Pinus densiflora. *Wood Sci. Technol.* **2020**, *54*, 123–137. [CrossRef]
32. *EN 14081-1:2005 + A1:2011*; Timber Structures—Strength Graded Structural Timber with Rectangular Cross Section—Part 1: General Requirements. National Standards Authority of Ireland: Glasnevin, Ireland, 2011.
33. *EN 1912*; Structural Timber—Strength Classes—Assignment of Visual Grades and Species. European Committee for Standardization (CEN): Brussels, Belgium, 2012.
34. *DIN 4074-1*; Sortierung von Holz nach der Tragfa ¨higkeit—Teil 1: Nadelschnittholz. Deutsches Institut Fur Normung E.V.: Berlin, Germany, 2012.
35. Hui, B.; Wen, G.; Zhao, Z.; Li, D. Line-scan camera calibration in close-range photogrammetry. *Opt. Eng.* **2012**, *51*, 053602. [CrossRef]
36. Kim, J.; Ahn, S.; Jeon, J.W.; Byun, J. A high-speed high-resolution vision system for the inspection of TFT LCD, ISIE 2001. In Proceedings of the ISIE 2001. 2001 IEEE International Symposium on Industrial Electronics Proceedings (Cat. No. 01TH8570), Pusan, Korea, 12–16 June 2001; Volume 1, pp. 101–105.
37. Wang, H. Implementing of microscopic images mosaic revising algorithm. *Graph. Signal Process.* **2011**, *3*, 56–63. [CrossRef]
38. Deng, L.; Li, J.; Han, Z. Online defect detection and automatic grading of carrots using computer vision combined with deep learning methods. *LWT* **2021**, *149*, 111832. [CrossRef]
39. Sun, W.-H.; Yeh, S.-S. Using the Machine Vision Method to Develop an On-machine Insert Condition Monitoring System for Computer Numerical Control Turning Machine Tools. *Materials* **2018**, *11*, 1977. [CrossRef]
40. Pahlberg, T.; Hagman, O.; Thurley, M. Recognition of boards using wood fingerprints based on a fusion of feature detection methods. *Comput. Electron. Agric.* **2015**, *111*, 164–173.
41. Xu, J.; Wu, X.; Liu, H.; Zhang, M. An optimization algorithm based on no-fit polygon method and hybrid heuristic strategy for irregular nesting problem. In Proceedings of the 2017 36th Chinese Control Conference (CCC), Dalian, China, 26–28 July 2017; Volume 36, pp. 2858–2863.
42. Rao, Y.; Wang, P.; Luo, Q. Hybridizing Beam Search with Tabu Search for the Irregular Packing Problem. *Math. Probl. Eng.* **2021**, *2021*, 5054916.
43. Wiedensohler, A.; Wiesner, A.; Weinhold, K.; Birmili, W.; Hermann, M.; Merkel, M.; Müller, T.; Pfeifer, S.; Schmidt, A.; Tuch, T.; et al. Mobility particle size spectrometers: Calibration procedures and measurement uncertainties. *Aerosol Sci. Technol.* **2018**, *52*, 146–164.
44. Wells, L.; Gazo, R.; Del Re, R.; Krs, V.; Benes, B. Defect detection performance of automated hardwood lumber grading system. *Comput. Electron. Agric.* **2018**, *155*, 487–495. [CrossRef]
45. Zhang, Z.; Liu, C.; Hu, F.; You, Y.; Hu, W.; Zhang, X. Are Both Preoperative Full-Spine 3Dimensional Computed Tomography Scans and X-ray Films Necessary for Patients with Ankylosing Spondylitis Kyphosis? *Orthop. Surg.* **2022**, *5*. [CrossRef]
46. Zhang, S. High-speed 3D shape measurement with structured light methods: A review. *Opt. Lasers Eng.* **2018**, *106*, 119–131. [CrossRef]
47. Wood, T.; Ramakrishnan, K.K.; Shenoy, P.; van der Merwe, J. CloudNet: Dynamic pooling of cloud resources by live WAN migration of virtual machines. *ACM Sigplan Not.* **2011**, *46*, 121–132.
48. Peng, M.; Ho, Y.; Wang, W.; Chui, Y.H.; Gong, M. Measurement of wood shrinkage in jack pine using three dimensional digital image correlation (DIC). *Holzforschung* **2012**, *66*, 639–643. [CrossRef]
49. Tu, Y.; Ling, Z.; Guo, S.; Wen, H. An Accurate and Real-Time Surface Defects Detection Method for Sawn Lumber. *IEEE Trans. Instrum. Meas.* **2021**, *70*, 1–11. [CrossRef]
50. Zeng, Y.; Xiang, H.; Zheng, N.; Cao, X.; Wang, N.; Wang, Z.L. Flexible triboelectric nanogenerator for human motion tracking and gesture recognition. *Nano Energy* **2022**, *91*, 106601. [CrossRef]